Interparticle Interactions and Magnetic Anisotropy in Cobalt Ferrite Nanoparticles: Influence of Molecular Coating

ARTICLE *in* CHEMISTRY OF MATERIALS · FEBRUARY 2012

Impact Factor: 8.35 · DOI: 10.1021/cm203280y

6 AUTHORS, INCLUDING:

Davide Peddis
Italian National Research Council
64 PUBLICATIONS **820** CITATIONS
SEE PROFILE

Carla Cannas
Università degli studi di Cagliari
100 PUBLICATIONS **1,717** CITATIONS
SEE PROFILE

Anna Musinu
Università degli studi di Cagliari
121 PUBLICATIONS **2,689** CITATIONS
SEE PROFILE

Giorgio Piccaluga
Università degli studi di Cagliari
141 PUBLICATIONS **3,406** CITATIONS
SEE PROFILE

CHEMISTRY OF MATERIALS

Article

pubs.acs.org/cm

Interparticle Interactions and Magnetic Anisotropy in Cobalt Ferrite Nanoparticles: Influence of Molecular Coating

Davide Peddis,* Federica Orrù, Andrea Ardu, Carla Cannas, Anna Musinu, and Giorgio Piccaluga

Dipartimento di Scienze Chimiche, Università di Cagliari, Cittadella U3niversitaria, 09042 Monserrato, Cagliari, Italy

Supporting Information

ABSTRACT: Molecular coating of nanoparticles represents probably the most important and, at the same time, critical step to design new nanostructured magnetic materials. The interaction between molecules and surface atoms leads to a strong modification of surface magnetic properties, that are one of the key points in the physics of magnetic nanoparticles. In this paper the magnetic properties of $CoFe_2O_4$ nanoparticles ($\langle D \rangle \cong 4-8$ nm) coated with oleic acid have been investigated in order to clarify the role of the molecular coating on the interparticle interactions and surface anisotropy. An increase of magnetic anisotropy (i.e., coercive field and anisotropy constant) with particle size is observed in coated nanoparticles, indicating that the magnetic anisotropy is governed mainly by its magneto-crystalline component. The removal of molecular coating induces a strong increase of anisotropy, because of the increase of its surface component, as indicated by the increase of exchange bias field.

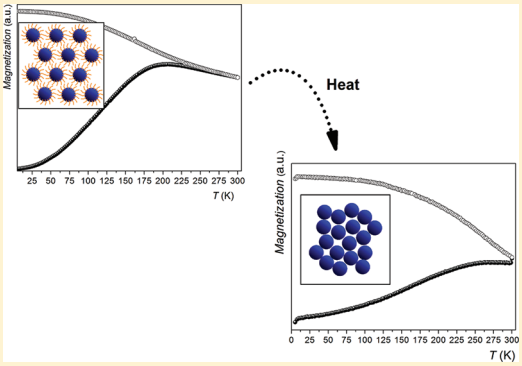

KEYWORDS: *cobalt ferrite, oleic acid, coated magnetic nanoparticles, surface anisotropy, interparticle interactions*

1. INTRODUCTION

Among the many applications of magnetic nanoparticles, those in biomedicine are particularly interesting and widespread. Generally speaking, the magnetic properties required for these applications are superparamagnetic behavior at room temperature, high saturation magnetization, size in the 1−50 nm range.[1,2] In addition, biocompatibility and functionalization requirements impose to coat the nanoparticles with a protective layer.[3,4] The coating substances may modify the magnetic properties of the core nanoparticles. In fact, they may induce variations in saturation magnetization[5] and, most of all, they may affect the energy barrier, ΔE_a, that the particle has to overcome to achieve a thermally activated transition from a blocked state under the blocking temperature, T_B, to a superparamagnetic state.

For particles with uniaxial anisotropy and easy axis aligned with the direction of external field, H, the energy barrier can be written as[6]

$$\Delta E_a = KV\left(1 \pm \frac{H}{H_K}\right)^2 \quad (1)$$

where

$$H_K = \frac{2K}{M_s} \quad (2)$$

Equations 1 and 2 show that ΔE_a can be generally considered proportional to the particle volume, V, and to the anisotropy constant, K. The anisotropy energy depends mainly on the structure and chemical composition of the material (i.e., magnetocrystalline and magnetostatic anisotropy). In addition, reducing particle size, the high surface to volume ratio can strongly influence the magnetic anisotropy (i.e., surface anisotropy). Magnetic properties at the particle surface are governed by the breaking of the lattice symmetry associated with several chemical and physical effects leading to a site-specific surface energy. Moreover, the interaction between molecules and surface atoms of nanoparticles can induce modification on surface anisotropy.[3,5,7] Then, in principle, the properties of the magnetic nanoparticles may be tailored by adapting their surface molecular coating.[8]

The magnetic behavior of a nanoparticle assembly can also be strongly affected by interparticle interactions that lead to an increase in the energy barrier.[9] The magnetic interactions can be due to dipolar and exchange coupling among nanoparticle surface atoms and play a fundamental role in the physics of these systems. Indeed, for application, concentrated assemblies of individually responding magnetic entities are required. This last requirement is difficult to be satisfied as interparticle dipole−dipole interactions are strongly enhanced by both an increase in the size of the magnetic nanoparticles and an increase of their concentration. Surface coating of the nanoparticles represents an useful tool in order to tune the interactions between nanoparticles, increasing the mean interparticle distance.

Comprehensive studies on this subject are rather poor and conflicting results have been presented. Berkowitz and co.,[10] in a pioneering work, showed as the presence of organic coating

Received: November 2, 2011
Revised: January 30, 2012
Published: February 22, 2012

leads to an increase of effective anisotropy, whereas more recently Vestal et al. showed in details as the organic coating can be used in order to reduce the coercivity.[8] It should be underlined that the systems studied by Berkowitz and Vestal have been prepared with different synthetic approaches. Berkowitz studied $NiFe_2O_4$ nanoparticles prepared by ball milling synthetic procedure, that usually leads to particles with irregular surface morphology and strong volume strain that can give rise to some surface and/or internal spin-canting.[11] In this paper, the increase in anisotropy has been mainly ascribed to the surfactant interactions with Ni^{2+} ion. On the other hand, Vestal et al. discussed the effect of molecular coating on magnetic properties of $MnFe_2O_4$ nanoparticles prepared by solution phase chemical methods (i.e., micellar method) that, because of the low synthesis temperature, lead to nanoparticles with low degree of crystallinity.

One the most interesting cases deals with particles coated with oleic acid. In fact, one of the most appealing synthesis procedure makes use of a solution reaction of metals acetylacetonates with 1,2-hexadecanediol in the presence of a mixture of oleic acid and oleylamine. The decomposition at high temperature of these organic precursors in organic solvents allows to obtain nanoparticles with various size and narrow size distribution, with a good control on structural and physical features of the materials.[12,13] Some magnetic studies on iron oxides coated with oleic acid have been reported[14−16] and they put into evidence the strong effect of the oleic acid coating on the magnetic properties. The high values of the saturation magnetization M_s, the reversible magnetic behavior at room temperature observed in particles about 17 nm large, the highest coercivity values for the largest particles have been interpreted in terms of the reduction of surface anisotropy due to a suppression of spin-canting and interparticle interactions due to the increase of particles separation. However, these studies cannot be considered conclusive, both because they investigated and compared particles not prepared by the same route, and because of some internal contradiction. For instance, some authors state that M_s does not vary with particle size,[14,15] whereas the opposite is reported in another paper.[17]

To go deeper in this subject, we investigated magnetic properties of cobalt ferrite particles, prepared by the method mentioned above[18] that, to the best of our knowledge, has not yet been studied from this point of view, with particular attention to the effect of the molecular coating on the interparticle interactions and magnetic anisotropy. In fact, cobalt ferrites are very attractive in the biomedical field for their high saturation magnetization and magnetic anisotropy, which give rise to suitable magnetic behavior at room temperature. Furthermore, bulk $CoFe_2O_4$ is characterized by a strong cubic anisotropy of magnetocrystalline origin, mainly due to the Co^{2+} ions, which have nonzero orbital momentum.[19] Entering in nanoscale, a coexistence of cubic and uniaxial anisotropy is observed, with a completely uniaxial anisotropy for particle size below 5 nm.[20]

To study the effect of the molecular coating on interparticle interactions and magnetic anisotropy in nanostructured cobalt ferrite, three samples with different particle size in the range ∼ 4−8 nm were prepared. The sample with the smallest particle size (i.e., higher surface/volume ratio) was submitted to 1 h thermal treatments at the selected temperatures of 350 and 500 °C, in order to evaluate the effect of the coating removal on the complex interplay between surface anisotropy and interparticle interactions.

2. EXPERIMENTAL SECTION

2.1. Synthesis. Three cobalt ferrite nanoparticles of different sizes (CoFe1, CoFe2, CoFe3) were synthesized by thermal decomposition of $Fe(acac)_3$ and $Co(acac)_2$ in the presence of oleic acid and oleylamine as surfactants and organic solvents with different boiling points.[13] All the samples were synthesized using iron (III) acetylacetonate (Janssen Chimica 99%, 2 mmol), cobalt(II) acetylacetonate (Janssen Chimica 99%, 1 mmol), 1,2-hexadecanediol (Aldrich 97%, 10 mmol), oleic acid (Aldrich 90%, 6 mmol), oleylamine (Aldrich <70%, 6 mmol). Phenyl ether (Aldrich 99%, 20 mL) for CoFe1 sample and benzylether (Aldrich 99%, 20 mL) for CoFe2, and CoFe3 samples were used as solvents; all the reagents were mixed into a three-neck, round-bottom flask and stirred magnetically. Under reflux, the mixtures were heated gradually to 200 °C and kept at this temperature for 30, 60, and 120 min for CoFe1, CoFe2, and CoFe3 respectively. The temperature was then increased rapidly up to 265 °C for CoFe1, and up to 295 °C for CoFe2 and CoFe3 samples and the mixtures were kept for 30 min, CoFe1 and CoFe2, and 60 min, CoFe3, at this temperature. During the process, the initial reddish-orange color of the solutions gradually changed to dark-black, indicating the formation of the oleyl-cobalt ferrite nanoparticles. The black-colored mixture was cooled to room temperature by removing the heat source. Ethanol (40 mL) was then added to the mixture and the black material was precipitated and separated via centrifugation. The black product was then dispersed in hexane or in cyclohesane and centrifugated once more to remove any undispersed residue, giving rise to a ferrofluid that retains its stability for several months. The nanoparticles were precipitated by addition of excess ethanol, separated and washed by centrifugation (4500 rpm, 15 min), to remove the solvent and dried at 40 °C overnight to evaporate alcohol residual. In Table 1, the key parameters of the synthesis are summarized.

Table 1. Key Parameters of the Synthesis Procedure

sample	solvent	thermal step 1	thermal step 2
CoFe1	phenyl ether	30 min at 200 °C	30 min at 265 °C
CoFe2	benzyl ether	60 min at 200 °C	30 min at 295 °C
CoFe3	benzyl ether	120 min at 200 °C	60 min at 295 °C

2.2. Experimental Techniques and Data Treatments. The samples were characterized by XRD, using a Seifert diffractometer with a $\theta-\theta$ Bragg−Brentano geometry with Cu−K_α wavelength. The mean dimension, $\langle D_{XRD}\rangle$, of the crystalline coherent domain (i.e., crystallite) was obtained by Scherrer's equation

$$\langle D_{XRD}\rangle = \frac{K\lambda}{\beta\cos\theta} \tag{3}$$

where K is a constant related to the crystallite shape (0.9) and β is the pure breath of the powder reflection free of the broadening due to instrumental contributions.

FTIR spectra were collected in the region from 400 to 3800 cm^{-1}, using a Bruker Equinox 55 spectrophotomer. Nanoparticles were analyzed dispersing powders in KBr pellets.

Finely ground samples were dispersed in octane and submitted to an ultrasonic bath. The suspensions were then dropped on carbon-coated copper grids for the TEM observations. Nanoparticles were observed in electron micrographs obtained with a TEM (JEOL 200CX), operating at 200 kV. HRTEM images were obtained with a JEM 2010 UHR equipped with a Gatan Imaging Filter (GIF) and a 794 slow scan CCD camera. Particle size distribution was calculated on about 200 nanoparticles in different images in bright field mode and fitted with a log-normal function

$$P(D) = \frac{100}{\langle D_{TEM}\rangle\,\sigma\,\sqrt{2\pi}}\exp-\left(\ln^2\frac{(D/\langle D_{TEM}\rangle)}{2\sigma^2}\right) \tag{4}$$

dx.doi.org/10.1021/cm203280y | Chem. Mater. 2012, 24, 1062−1071

Mean particle diameter $\langle D_{TEM}\rangle$ and polydispersity ($\sigma \times 100$) are reported in Table 2. DC magnetization measurements were performed

Table 2. Mean Particle Size from XRD Pattern ($\langle D_{XRD}\rangle$), Mean Particle Size from TEM Data ($\langle D_{TEM}\rangle$), Polydispersity (σ), Temperature Corresponding to the Maximum in ZFC Curve (T_{max}), Irreversibility Temperature (T_{irr}), Blocking Temperature from TRM Measurement (T_B)[a]

sample	$\langle D_{XRD}\rangle$ (nm)	$\langle D_{TEM}\rangle$ nm	σ (%)	T_{max} (K)	T_{irr} (K)	T_B (K)
CoFe1	5.0(2)	4.6(1)	26(1)	207(5)	247(5)	120(3)
CoFe2	6.3(3)	6.5(1)	13(1)	224(4)	285(4)	154(4)
CoFe3	7.8(3)	7.8(2)	10 (1)	262(5)	283(2)	200(3)

[a]Uncertainties in the last digit are given in parentheses.

with a Quantum Design SQUID magnetometer, equipped with a superconducting coil which produces magnetic fields in the range from −5 T to +5 T. The samples in form of powders were immobilized in an epoxy resin to prevent any movement of the nanoparticles during the measurements. Magnetization versus temperature measurements were performed using the zero-field-cooled (ZFC), field-cooled (FC), and thermoremanent magnetization (TRM) protocols. Zero-field-cooled and field-cooled magnetization measurements were carried out by cooling the sample from room temperature to 5 K in zero magnetic field; then a static magnetic field of 2.5 mT was applied. M_{ZFC} was measured during warming up from 5 to 300 K, whereas M_{FC} was recorded during the subsequent cooling. In the TRM measurements, the sample was cooled from 300 to 5 K in an external magnetic field of 2.5 mT; the field was then turned off and the magnetization was measured on warming up. The field dependence of remanent magnetization was measured using the IRM (isothermal remanent magnetization) and DCD (direct current demagnetization) protocols. The initial state for an IRM measurement is a totally demagnetized sample cooled in a zero magnetic field. In the present case, an external field was applied for 10 s, then it was switched off and the remanence was measured (M_{IRM}). The process was repeated, increasing the field up to 5T. In a DCD measurement the initial state is the magnetically saturated one. An external field of −5 T was applied for 10 s, and then a small external field in the direction opposite to magnetization was applied; after 10 s, it was switched off and the remanent magnetization (M_{DCD}) was measured. This was repeated increasing the field up to +5T.

3. RESULTS AND DISCUSSION

The X-ray diffraction patterns of the synthesized powders are shown in Figure 1; Bragg reflections in the 2θ range of 10−70° correspond to those of a single $CoFe_2O_4$ phase with a cubic spinel structure (PDF Card 22−1086). No peak of any other phase was detected. Using Debye−Scherrer formula on [400] reflection, the size of crystalline coherent domains was obtained (Table 2), showing that the used synthesis conditions are efficient in the variation of crystallite size.

TEM analysis (Figure 2a−c) clearly indicates that thermal decomposition of iron/cobalt-organic precursor in an organic media leads to the formation of essentially spherical and uniform nanoparticles. These nanoparticles self-assembled in hexagonal close-packed superlattice, due to the high degree of uniformity in diameter.[18] The presence of surfactants at the nanoparticle surface keeps them isolated from each other by a coating layer of about 2 nm. This is in agreement with thermal analysis results (see Figure S1 in the Supporting Information), indicating that weight percentage in oleic acid was between 22 and 30%. These are the weight percentages that correspond to a monolayer of oleic acid (molecule length, 1.97 nm; surface occupied by one molecule, 0.2 nm^2) molecules adsorbed on

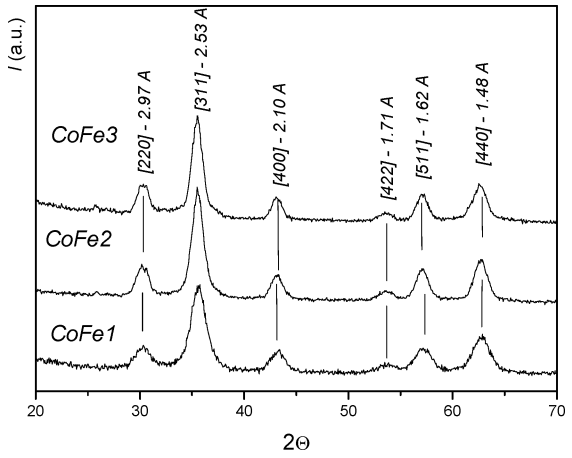

Figure 1. XRD patterns of CoFe1, CoFe2, and CoFe3 samples.

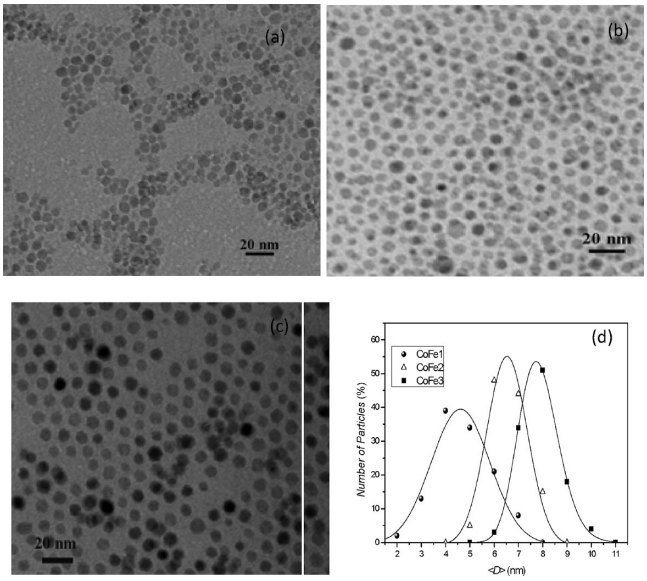

Figure 2. Bright-field images at low magnification for (a) CoFe1, (b) CoFe2, and (c) CoFe3; (d) particle size distributions obtained by TEM analysis.

the surface of nanoparticles with diameters in the explored range.[15]

Particle size distributions (symbols in Figure 2d), well fitted by log-normal functions for all the samples (lines in Figure 2d), lead to a measured mean diameter of 4.6, 6.5, and 7.8 nm for CoFe1, CoFe2, and CoFe3 samples, respectively (Table 2). The good agreement between $\langle D_{XRD}\rangle$ and $\langle D_{TEM}\rangle$ values indicates that all the samples show an high degree of cristallinity. A decrease of polydispersity is observed increasing particle size and this can be directly correlated with the synthesis procedure. Indeed, in order to obtain different particle size CoFe1, CoFe2, and CoFe3 starting mixtures were first heated at 200 °C for 30 min, 1 h, and 2 h. The observed inverse proportion between polydispersity and time length of the first thermal step at 200 °C confirms the suggestions reported in the literature, indicating as better monodispersion can be obtained increasing the time length of the first thermal step at 200 °C.[13]

In order to evaluate the effect of the surfactant on the interparticle interactions and on the magnetic anisotropy, the sample CoFe1 was submitted to thermal treatments at 350 °C

dx.doi.org/10.1021/cm203280y | Chem. Mater. 2012, 24, 1062−1071

($CoFe1_{T350}$) and 500 °C ($CoFe1_{T500}$) for 1 h. XRD patterns (see Figure S2a in the Supporting Information) indicate that the thermal treatments do not induce any structural change and only the cubic $CoFe_2O_4$ phase is still present in the samples. Debye–Scherer analysis on [400] reflection indicates that mean crystallite size in $CoFe1_{T350}$ is almost unchanged, whereas an increase in $\langle D_{XRD} \rangle$ is observed in $CoFe1_{T500}$ (Table 4). HRTEM analysis on $CoFe1_{T350}$ sample (Figure 3a,b) shows some coalescence of nanoparticles, with the presence of a small fraction of carbonaceous residual between them. Thermal treatment at 500 °C leads to the total decomposition of these residuals, inducing strong coalescence between nanoparticles (Figure 3c). However, the coalesced particles do not form bigger single crystal; in fact, two originally separated particles show the easily visible grain boundaries[21] (Figure 3d). There is no evidence of residual carbon at the grain boundaries, as shown in $CoFe1_{T350}$ sample. Because HRTEM indicates that residual carbon is absent in $CoFe1_{T500}$, its percentage in $CoFe1_{T350}$ sample can be estimated as the weight loss between 350 and 500 °C determined by thermal analysis (0.6%). This indicates that also at 350 °C the oleic acid can be considered almost completely decomposed. This is confirmed by IR measurements reported in Figure S2b in the Supporting Information. The spectrum of CoFe1 sample contains modes characteristic of oleic group: the peaks at 2855 and 2931 cm^{-1} are due to the symmetric and antisymmetric CH_2 stretching modes and the modes at 1554 and 1412 cm^{-1} arise from the ν_a ($-COO^-$) and ν_s ($-COO^-$). All these signals disappear in the spectra of the thermally treated samples, indicating that the thermal treatment allows the surfactant elimination.

3.1. Magnetic Properties: Effect of Particles Size. Temperature dependence of magnetization was investigated by ZFC, FC, and TRM protocols. Figure 4a–c show ZFC and FC magnetization curves of CoFe1, CoFe2 and CoFe3 samples, respectively. All the samples show a qualitatively similar behavior: ZFC curves exhibit a maximum, and the corresponding temperature (T_{max}) is directly proportional to the average blocking temperature, with a proportionality constant ($\beta = 1-2$) depending on the type of T_B distribution.[22] An irreversible magnetic behavior is observed below a given temperature (T_{irr}) that is related to the blocking of the biggest particles.[23,24] Going to lower temperatures the FC curves show a temperature-independent behavior, indicating the presence of long-range magnetic interparticle interactions that lead to a magnetic ordered state with high anisotropy.[25,26] As expected, T_{max} and T_{irr} (table 2) increase with particle size; this can be due to an increase of volume anisotropy and of interparticle interactions. TRM magnetization curves of the CoFe1, CoFe2, and CoFe3 samples are reported in Figure 4d–f (full symbols), respectively. For all the samples, M_{TRM} decreases with increasing temperature, as expected for an assembly of magnetic monodomain particles. For noninteracting particles, the

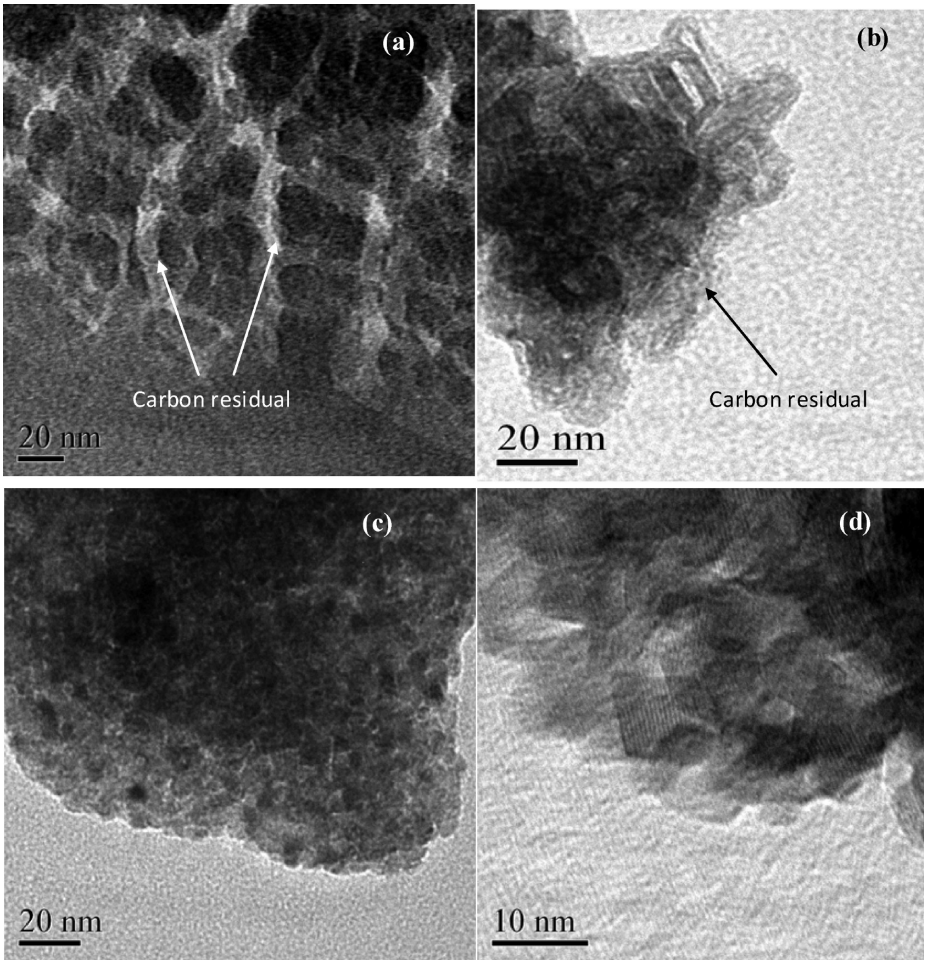

Figure 3. HRTEM images of (a, b) $CoFe1_{T350}$ and (b, d) $CoFe1_{T500}$ samples.

dx.doi.org/10.1021/cm203280y | *Chem. Mater.* 2012, 24, 1062–1071

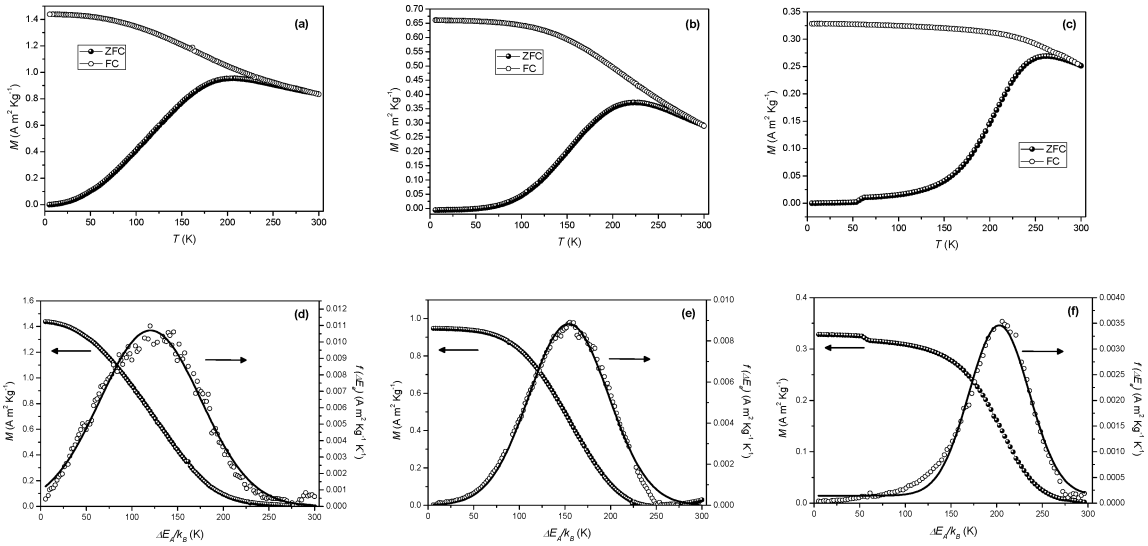

Figure 4. Upper part: ZFC (full symbols) and FC (empty symbols) DC magnetizations for (a) CoFe1, (b) CoFe2, and (c) CoFe3 samples; lower part TRM measurements (a) and corresponding distribution of magnetic anisotropy energies for (d) CoFe1, (e) CoFe2, and (f) CoFe3 samples.

derivative of M_{TRM} with respect to the temperature gives an estimate of the anisotropy energy barrier distribution[27]

$$f(\Delta E_a) \propto -\frac{dM_{TRM}}{dT} \quad (5)$$

In our samples, the derivative of M_{TRM} can actually be considered only as an indication of the ΔE_a distribution, because the role of the interparticle interactions on the physical behavior of the samples cannot be disregarded. Figure 4d–f shows the ΔE_a distribution (empty symbols) for each sample. Within the Néel model, the blocking temperature can be defined as the temperature at which the relaxation time is equal to the measuring time of the experimental technique. In practice, samples of small particles always exhibit particle size distribution, and often T_B is defined as the temperature at which 50% of the nanoparticles are in the superparamagnetic state.[28] We can obtain an estimate of the blocking temperature from the distribution of the magnetic anisotropy energy barriers by evaluating the temperature at which 50% of the particles overcome their anisotropy energy barriers (table 2). T_B values follow the same trend of T_{max} and T_{irr}. All the distributions of magnetic anisotropy can be satisfactory reproduced by Gaussian function (continuous line in Figure4f). Going from the CoFe1 to the CoFe3 sample, a decrease in magnetic anisotropy distribution wideness is observed, reflecting the decrease of the particle size polydispersion shown by TEM analysis.

Field dependence of magnetization was studied at low temperature (figure 5) and saturation magnetization (M_s), reduced remanent magnetization (M_r/M_s) and coercive field (H_c) extracted from hysteresis loops are reported in Table 3. Saturation magnetization is almost independent of particles size, as reported for Fe_3O_4 nanoparticles prepared with the same synthesis method.[15] On the other hand, reduced remanent magnetization increases with the increase of particles size ranging from 0.68 to 0.88. These so high values of M_r/M_s suggest a tendency toward cubic anisotropy with the increase of particle size, the values for CoFe2 (0.81) and CoFe3 (0.88) being very close to theoretical values for $CoFe_2O_4$ particles with cubic anisotropy where $K_1 > 0$ (0.83) and $K_1 < 0$ (0.87).[29,30] This result is consistent with a study of $CoFe_2O_4$ nanoparticles,[20] where it was found that the M_r/M_s ratio increases as the mean particles size increases, indicating that the magnetic anisotropy changes from uniaxial to cubic symmetry. Coercivity values increase as the particle sizes increase from 1.29 T for CoFe1 samples to 1.81 T for CoFe3 sample. All the samples show high irreversibility field, with magnetizing and demagnetizing branches separated up to 3 T. Taking this splitting point as an estimate of the anisotropy field H_K,[31] it is possible to obtain the mean value of the effective anisotropy constant $\langle K_{eff} \rangle$ according to equation (2)[32] (we have taken H_K as the field where the difference between magnetizing and demagnetizing branches, normalized to M_s value becomes smaller than 3%). Both H_K and $\langle K_{eff} \rangle$ (Table 3) increase with the particle size, in agreement with the trend of coercivity. The trend of H_c, H_K, and $\langle K_{eff} \rangle$ indicates that magnetic anisotropy increases with the increase of particle size, as already observed for Fe_3O_4 nanoparticles in the particle size range 5–11 nm,[15] suggesting that surface component of anisotropy plays a minor role in these systems.

3.2. Interparticle Interactions. To get more information about quasi static magnetic properties of the materials, the dependence of remanent magnetization, recorded with DCD and IRM protocols, was investigated at low temperature (5 K). In the inset of Figure 6 are reported $M_{DCD}(H)/M_{sat}$ (full symbols) and $M_{IRM}(H)/M_{sat}$ (empty symbols) for all the samples. The increase of $M_{DCD}(5T)/M_{sat}$ and $M_{IRM}(5T)/M_{sat}$ confirms the tendency toward magnetic anisotropy with cubic symmetry with the increase of particle size.[33]

The analysis of remanent magnetization curves measured by IRM and DCD protocols allowed also to investigate the interaction regime among particles. For an assembly of non-interacting single-domain particles with uniaxial anisotropy and magnetization reversal by coherent rotation, the two remanence curves are related via the Wohlfarth equation

$$m_{DCD}(H) = 1 - 2m_{IRM}(H) \quad (6)$$

where $m_{DCD}(H)$ and $m_{IRM}(H)$ represent the reduced terms $M_{DCD}(H)/M_{DCD(5T)}$ and $M_{IRM}(H)/M_{IRM(5T)}$ and $M_{DCD(5T)}$ and $M_{IRM(5T)}$ are the remanence values for the DCD and IRM curves at 5 T, respectively.

dx.doi.org/10.1021/cm203280y | Chem. Mater. 2012, 24, 1062–1071

Following equation (6), the two irreversible susceptibilities ($\chi_{irr} = dm/dH$) are related as

$$\left|\frac{dm_{DCD}}{dH}\right| = 2\frac{dm_{IRM}}{dH} \quad (7)$$

with a maximum at the same reverse field. Deviations from such behavior are due to the presence of interactions which can be quantified in terms of the so-called interaction field

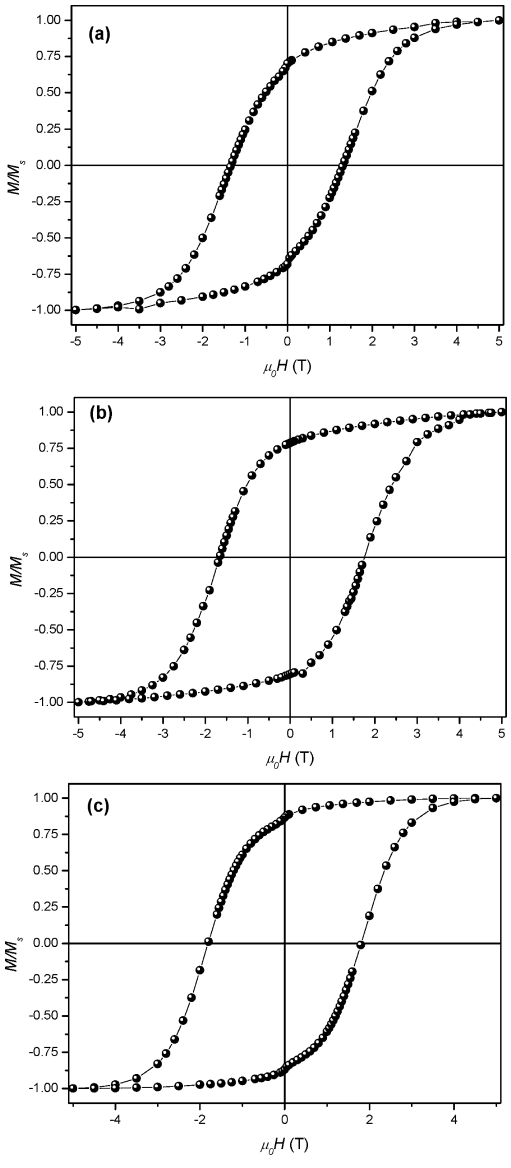

Figure 5. hysteresis loops recorded at 5K for (a) CoFe1, (b) CoFe2, and (c) CoFe3 samples

$$H_{int} = \frac{(H'_r - H_r)}{2} \quad (8)$$

H'_r and H_r correspond to the position of the maxima of the field derivative of $m_{DCD}(H)$ and $m_{IRM}(H)$ curves (i.e., maxima in the irreversible susceptibility which maps the switching field distribution). H_{int} values (Table 3) suggest weak demagnetizing interactions, increasing with particle size. In a sample of randomly distributed nanoparticles with average magnetic moment μ and average separation d, the energy due to dipole−dipole interactions for one particle is on the order of[24,34]

$$E_{dip} \approx \frac{\mu_0}{4\pi}\frac{\mu^2}{d^3} \quad (9)$$

Assuming a point dipole model (i.e., center to center maximum distance), a mean value of dipolar energy E_d/k_B (Table 3) has been calculated using equation 9 and defining the magnetic moment of a single domain particle as $\mu = M_s \times V$. An increase of dipolar energy is observed going from CoFe1 to CoFe3 sample. This effect can be ascribed mainly to a volume effect (i.e.: increase of μ), because the interparticle separation is equal in all the samples due to the molecular coating.[18] This is reflected by the M_{FC} magnetizations (Figure 4a−c) that show a temperature independent behavior below a certain temperature that increases with the increase of interparticle interactions. In addition, it is important to underline that, for all the samples, E_{dip}/k_B is well lower than T_B, indicating that superparamagnetic relaxation is mainly governed by magnetic anisotropy energy of the nanoparticles, suggesting a Vogel-Fulcher scenario.[35]

In order to clarify the role of the surfactant, the evolution of interparticle interactions with thermal treatments has been investigated. Kelly et al.[26] rewrote the Wohlfart relation (eq 6) to explicitly reveal deviations from a noninteracting case:

$$\Delta M = M_{DCD} - (1 - 2M_{IRM}) \quad (10)$$

In particular, a negative deviation from the linearity condition is an evidence of the predominance of dipole−dipole interactions, while a positive deviation can be attributed to the predominance of exchange interactions. ΔM plots indicate for all the samples (figure 7) the prevalence of dipolar-dipolar interactions, indicating that the thermal treatments up to 500 °C do not induce exchange coupling between particle surface.

For CoFe1 sample, ΔM peak (ΔH_p) is centered at 1,25 T, while for $CoFe1_{T350}$ and $CoFe1_{T500}$, ΔM amplitude (i.e., strength of interparticle interactions) is larger and ΔM peak shifted to higher fields ($\Delta H_p \cong 2.25$ T). The relative increase of amplitude ($CoFe1_{T350}/CoFe1 \cong 2.3$ and $CoFe1_{T500}/CoFe1_{T350} \cong 1.2$) indicates that, as expected, the molecular coating (i.e., increase of interparticle distance) play a major role in tuning the interparticle interactions with respect to increase of particle volume (i.e., increase of nanoparticle moment). This trend is confirmed by using equation 9. Despite similar particle size

Table 3. Mean Particle Size from XRD Pattern ($\langle D_{XRD}\rangle$), Saturation Magnetization (M_s), Reduced Remanent Magnetization (M_r/M_s), Coercive Field ($\mu_0 H_c$), Anisotropy Constant (K), Remanence Coercivity ($\mu_0 H_r$), Exchange Bias Field ($\mu_0 H_{ex}$), Interaction Field (H_{int}), Interaction Dipolar Energy (E_{dip})[a]

sample	$\langle D_{XRD}\rangle$ (nm)	M_s (A m^2 Kg^{-1})	M_r/M_s	$\mu_0 H_c$ (T)	$\mu_0 H_k$ (T)	K ($\times 10^5$) (J/m^3)	$\mu_0 H_r$ (T)	$\mu_0 H_{ex}$(mT)	$\mu_0 H_{int}$ (mT)	E_{dip} (K)
CoFe1	5.0(2)	70(2)	0.68	1.29(3)	4.30 (4)	7.47 (3)	1.60 (3)	−10	−60	8.0(5)
CoFe2	6.0(3)	68(2)	0.81	1.71(2)	4.48 (4)	7.79 (2)	1.90 (3)	−2.8	−78	37(2)
CoFe3	7.6(3)	67(2)	0.88	1.81 (4)	4.64 (5)	8.07 (3)	1.97 (4)	0	−79	60(3)

[a]Uncertainties in the last digit are given in parentheses.

dx.doi.org/10.1021/cm203280y | Chem. Mater. 2012, 24, 1062−1071

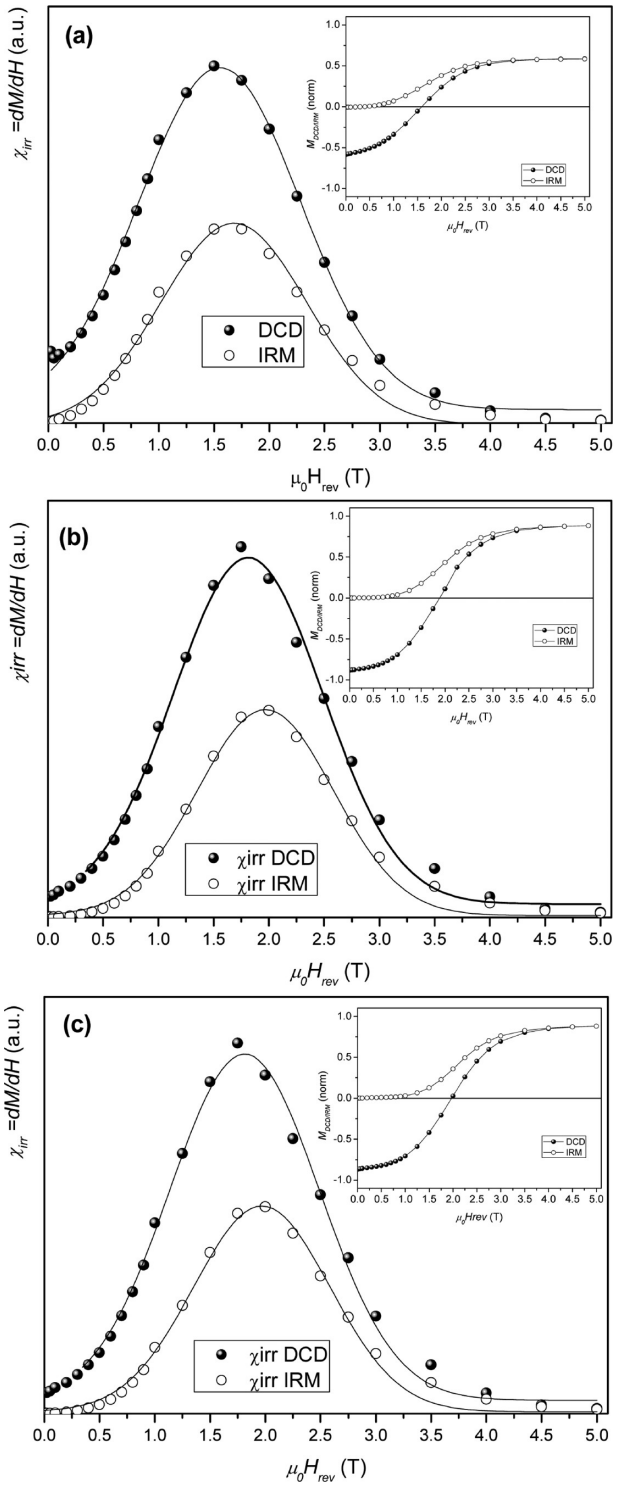

Figure 6. Irreversible susceptibility ($\chi_{irr} = dM/dH$) derived by DCD (full circles) and IRM (open circles) for the sample (a) CoFe1, (b) CoFe2, and (c) CoFe3 samples; insets: DCD and IRM curves.

$CoFe1_{T350}$ has a mean dipolar energy 18 times higher than CoFe1 sample, whereas only an increase of 1.85 is observed going from $CoFe1_{T350}$ to $CoFe1_{T500}$. On the other hand, the strong increase of ΔH_p due to thermal treatments and equal, within the experimental error, in samples $CoFe1_{T350}$ and $CoFe1_{T500}$, induces to believe that the decomposition of surfactant leads to a strong increase of magnetic anisotropy of the nanoparticles.

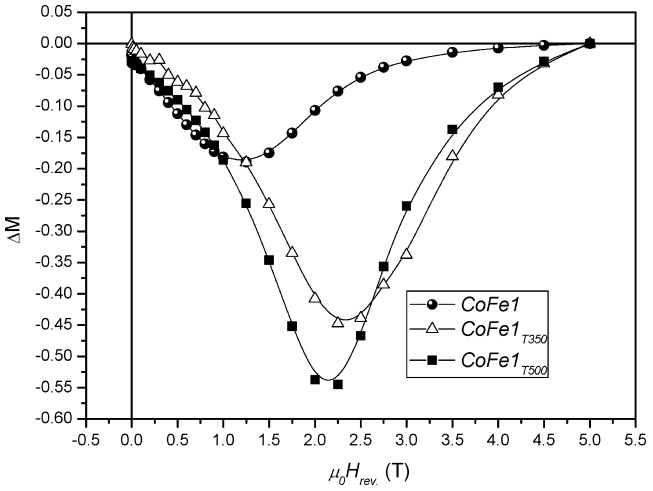

Figure 7. ΔM plot for the CoFe1 (full circles), $CoFe_{T350}$ (empty triangles), and $CoFe1_{T500}$ (full square) samples.

The combined increase of particle size and interparticle interactions induces a strong increase of the mean blocking temperature, as confirmed by ZFC FC measurements (see Figure S3 in the Supporting Information) that show T_{max} upon 300 K for $CoFe1_{T350}$ and $CoFe1_{T500}$ samples. The temperature independent behavior of M_{FC}, confirms this picture, indicating an increase of interparticle interactions going from CoFe1 to $CoFe1_{T500}$ sample.

3.3. Magnetic Anisotropy. Entering the nanoscale, the surface component (K_s) plays the key role in regulating the magnetic anisotropy of nanoparticles. Usually magnetic anisotropy increases with decreasing of particle size due the increase of K_s. On the contrary, a first investigation of magnetic properties suggests that in our systems anisotropy increases with increasing particle size, indicating that magnetocrystalline component plays the major role, as already observed in Fe_3O_4 nanoparticles prepared with the same synthesis method.[15−17] To put in evidence the occurrence of surface anisotropy, hysteretic behavior was investigated in more detail. Hysteresis loops at 5K were measured after cooling the samples in a field of 2 T (empty symbol in Figure 8) from room temperature. For the CoFe1 and CoFe2 samples, a shift of the loop along the field axis (higher for smaller particles) is observed after field cooling, whereas the loop remains symmetric with respect to the origin for the sample CoFe3. The shift of the loop, usually quantified as the exchange bias field (defined as $H_{ex} = -(H_{right} + H_{left})/2$) was already observed in ferrimagnetic nanoparticles.[36,37] It can be ascribed to the presence of a magnetically disordered spin structure at the surface (i.e., spin-canting), exchange coupled with a ferrimagnetically ordered core.[36−38] Interface exchange coupling is absent in biggest particles (CoFe3 sample) and in CoFe2 and CoFe1 samples H_{ex} increases with the decrease in particle size, because of the increase of surface/volume ratio (S/V). This leads to an increase of surface component of anisotropy, as indicated also by the increase of the slope at 5T, $(dM/dH)_{5T}$, with decreasing of particle size (Table 3). However, despite an increase in K_s, no effect on the macroscopic properties of the materials is observed (i.e., H_c, H_K, $\langle K_{eff} \rangle$ increase with particle size), indicating that the surface anisotropy is not the prevailing term. In order to clarify the role of the molecular coating in our systems, the evolution of magnetic properties with thermal treatments for the sample CoFe1 appears extremely useful. Only a small variation of saturation magnetization is observed in

dx.doi.org/10.1021/cm203280y | Chem. Mater. 2012, 24, 1062−1071

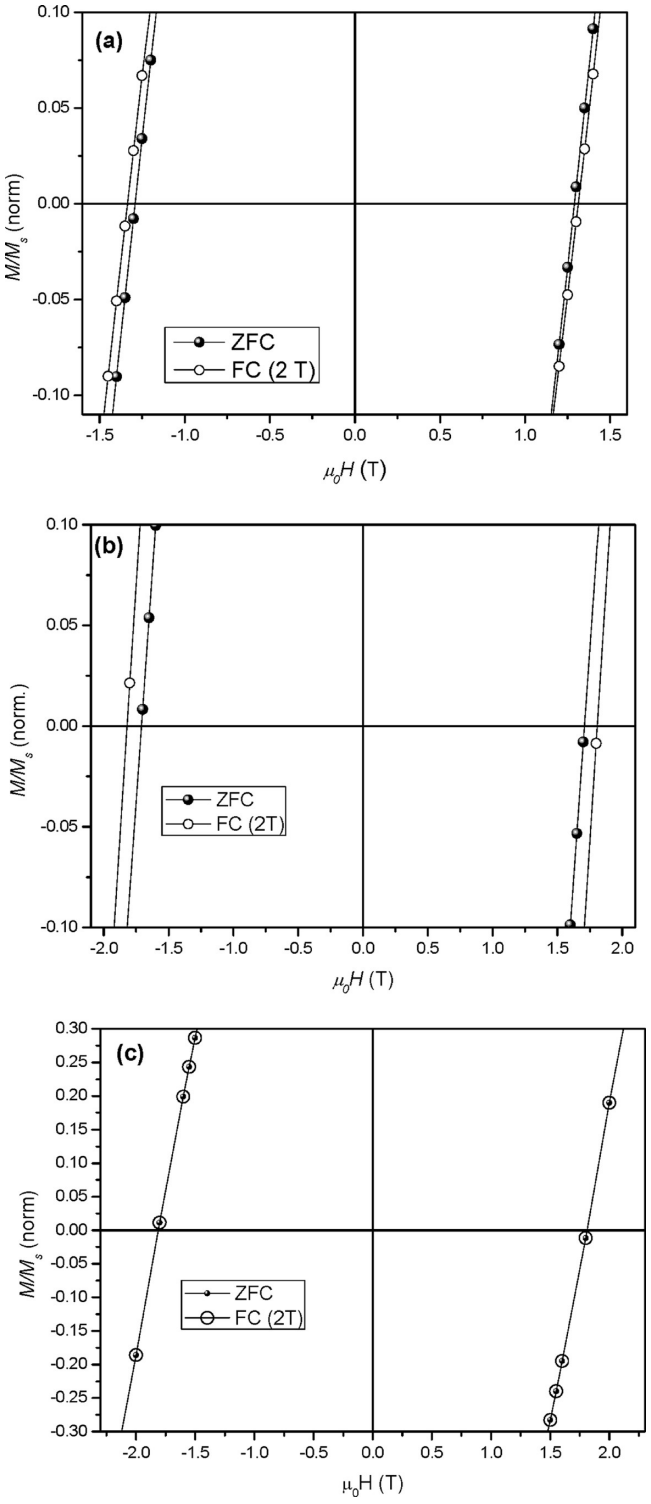

Figure 8. Details of hysteresis loops recorded at 5 K after zero field cooling (full symbols) and after cooling the sample under field (empty symbols) from 300 K. The cooling field was 2 T.

$CoFe1_{T350}$ and $CoFe1_{T500}$ (Table 4) that is compatible with very small variation in cationic distribution due to the effect of thermal treatment.[11,28] In figure 9a $(dM/dH)_{5T}$ as a function of the surface volume ratio is reported. For the coated samples the increase $(dM/dH)_{5T}$ has a monotonic linear dependence by S/V, whereas thermal treatments lead to a strong increase of the slope at high field. This clearly indicates that the decomposition of the

Table 4. Mean Particle Size from XRD Pattern ($\langle D_{XRD}\rangle$), Interaction Dipolar Energy (E_{dip}), Saturation Magnetization (M_s) coercive field ($\mu_0 H_c$)[a]

sample	$\langle D_{XRD}\rangle$ (nm)	E_{dip} (K)	M_s (A m^2 Kg^{1-})	$\mu_0 H_c$ (T)
CoFe1	5.0(2)	8.0(5)	70(2)	1.29(3)
$CoFe1_{T350}$	5.5(3)	144(4)	78(4)	1.93(4)
$CoFe1_{T500}$	7.3(3)	267(7)	72(3)	1.82(3)

[a]Uncertainties in the last digit are given in parentheses.

oleic acid induces a strong increase of the surface component of anisotropy, revealing the key role played by the molecular coating. In nanoparticles the coordination symmetry is greatly reduced for metal cations at the surface due to the missing of some oxygen atoms and oleic acid can be viewed as effectively taking the position of the missing atoms. Upon the basis of ligand field theory, the ligand coordination provides the crystal field splitting energy (CFSE) generated from *d* orbitals splitting with a magnitude determined by the ligands at a given coordination symmetry. Magnetic anisotropy is generated by the spin−orbit coupling occurred at magnetic cations, and the anisotropy decreases with decreasing spin−orbit coupling. When metal cations at the surface of nanoparticles are coordinated with oleic acid, CFSE results larger and the spin−orbit coupling becomes smaller. Consequently the surface anisotropy decreases and the coercivity of nanoparticle is reduced (table 4). This appears evident by the strong increase of $(dM/dH)_{5T}$ shown by the sample $CoFe1_{T500}$ with respect to CoFe2 sample, despite they have similar S/V ratio. The increase of surface component of anisotropy, observed in thermal treated samples, is reflected in an increase of the effective anisotropy of the materials as revealed by the increase of H_c. The increase in surface component of anisotropy is qualitatively reflected by H_{ex} (Figure 9b) that also increases with the thermal treatments. In fact, surface usually exhibits some degree of spin disorder but the presence of oleic acid makes the symmetry and crystal field of the surface metal ion more closely resembling that of the core. Therefore the presence of covalent bounded molecular coating[18] reduces the spin disorder (i.e surface anisotropy), hindering interface exchange coupling between ordered core and magnetically disordered shell. This explains the strong increase of H_{ex} observed in $CoFe1_{T350}$ sample, while the further small increase of exchange bias field in the sample $CoFe1_{T500}$ can be ascribed to the increase of interparticle interactions that improves the efficiency of exchange bias phenomenon.[39]

4. CONCLUSIONS

Molecular coating of nanoparticles represents probably the most important and, at the same time, critical step in order to design new nanostructured magnetic materials. The interactions between molecules and surface atoms leads to a strong modification of surface anisotropy and interparticle interactions, that are two of the main interconnected factors that govern the physics of an assembly of magnetic particles. Within this complex framework, a deep magnetic investigation on $CoFe_2O_4$ nanoparticles, coated by oleic acid covalently bounded at the particle surface,[18] has been carried out in order to clarify the role of molecular coating . Surprisingly, the evolution of magnetic properties shows an increase of magnetic anisotropy with particle size in the range 4−8 nm, indicating that in these systems the surface component of the anisotropy plays a secondary role with respect to magnetocrystalline component. By thermal treatments at selected temperature

dx.doi.org/10.1021/cm203280y | *Chem. Mater.* 2012, 24, 1062−1071

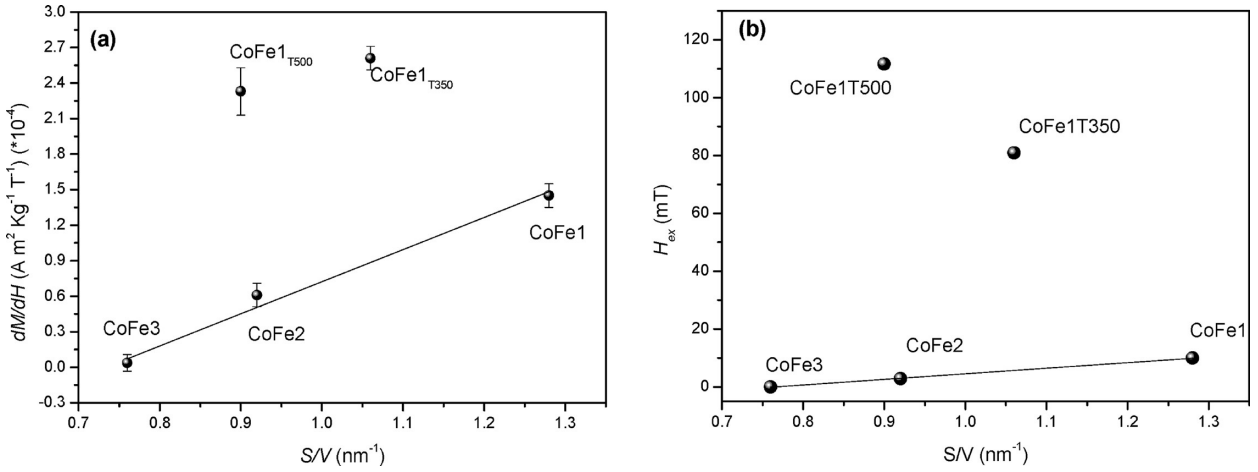

Figure 9. (a) High field slope, $(dM/dH)_{ST}$, and (b) exchange bias field, H_{ex}, as a function of surface/volume ratio, S/V.

(350−500 °C) on the sample with smaller particle size (i.e., higher S/V ratio), the effect of molecular coating on interparticle interactions and magnetic anisotropy was investigated. Structural and morphological characterization (XRD, TEM, thermal analysis, and FT-IR) indicates that at 350 °C all the surfactant has been decomposed, reducing the interparticle distance, without sensible variation of particle size. The treatment at 500 °C induces an increase of particle size (i.e., magnetic moment of nanoparticle) and it induces some interparticle coalescence. The magnetic characterization of the thermally treated samples shows relevant differences between CoFe1 and $CoFe1_{T350}$, while only small differences are observed between $CoFe_{T350}$ and $CoFe_{T500}$. As expected, a strong increase of interparticle interactions is observed in $CoFe1_{T350}$ due to the elimination of surfactant (i.e., reduction of interparticle distance), whereas the increase of particle size (i.e., magnetic moment of nanoparticle) induces only small variation of interparticle interactions. The strong increase of the field corresponding to ΔM peak (ΔH_p) in samples without surfactant is a clear indication that the elimination of molecular coating induces an increase of magnetic anisotropy, as confirmed by the increase of H_c, H_K, and $\langle K_{eff} \rangle$. The presence of interface exchange coupling between ferromagnetically ordered core and magnetically disordered shell, with H_{ex} that is appreciably higher in thermally treated samples, clearly indicates that the increase in anisotropy is due to its surface component, which recovers the main role when the surfactant has been removed.

■ ASSOCIATED CONTENT

Supporting Information

Additional figures (PDF). This material is available free of charge via the Internet at http://pubs.acs.org.

■ AUTHOR INFORMATION

Corresponding Author

*E-mail: dpeddis@hotmail.com

Notes

The authors declare no competing financial interest.

■ ACKNOWLEDGMENTS

D.P. was granted by RAS (Regione Sardegna−Centro regionale di Programmazione) cofounded by PO Sardegna FSE 2007-2013, L.R.7/2007 "Promozione della ricerca scientifica e dell'innovazione tecnologica in Sardegna". The authors thank Dr. G. Muscas for assistance in magnetic measurements and useful discussion

■ REFERENCES

(1) Pankhurst, Q. A.; Connelly, J.; Jones, S. K.; Dobsonb, J. *J. Phys. D: Appl. Phys.* **2003**, *36*, R167−R181.

(2) Suber, L.;Peddis, D. Approaches to Synthesis and Characterization of Spherical and Anisometric Metal Oxide Magnetic Nanomaterials. In *Magnetic Nanomaterials*; Wiley: Weinheim, Germany, 2010; Vol. *4*.

(3) Lu, Y.; Yin, Y.; Mayers, B. T.; Xia, Y. *Nano Lett.* **2002**, *2*, 183−186.

(4) Davies, R.; Schurr, G. A.; Meenan, P.; Nelson, R. D.; Bergna, H. E.; Brevett, C. A. S.; Goldbaum, R. H. *Adv. Mater.* **1998**, *10*, 1264−1270.

(5) Tanaka, Y.; Saita, S.; Maenosono, S. *Appl. Phys. Lett.* **2008**, *92*, 7.

(6) El-Hilo, M.; O'Grady, K.; Chantrell, R. W. *J. Magn. Magn. Mater.* **1992**, *114*, 307−313.

(7) Bødker, F.; Mørup, S.; Linderoth, S. *Phys. Rev. Lett.* **1994**, *72*, 282−285.

(8) Vestal, C. R.; Zhang, Z. J. *J. Am. Chem. Soc.* **2003**, *125*, 9828−9833.

(9) Parker, D.; Dupuis, V.; Ladieu, F.; Bouchaud, J. P.; Dubois, E.; Perzynski, R.; Vincent, E. *Phys. Rev. B* **2008**, *77*, 104428−104429.

(10) Berkowitz, A. E.; Lahut, J. A.; Jacobs, I. S.; Levinson, L. M.; Forester, D. W. *Phys. Rev. Lett.* **1975**, *34*, 594−597.

(11) Peddis, D.; Mansilla, M. V.; Mørup, S.; Cannas, C.; Musinu, A.; Piccaluga, G.; Orazio, F.; Lucari, F.; Fiorani, D. *J. Phys. Chem. B* **2008**, *112*, 8507−8513.

(12) Sun, S.; Zeng, H. *J. Am. Chem. Soc.* **2002**, *124*, 8204−8205.

(13) Sun, S.; Zeng, H.; Robinson, D. B.; Raoux, S.; Rice, P. M.; Wang, S. X.; Li, G. *J. Am. Chem. Soc.* **2004**, *126*, 273−279.

(14) Guardia, P.; Batlle-Brugal, B.; Roca, A. G.; Iglesias, O.; Morales, M. P.; Serna, C. J.; Labarta, A.; Batlle, X. *J. Magn. Magn. Mater.* **2007**, *316*, e756−e759.

(15) Roca, A. G.; Morales, M. P.; O'Grady, K.; Serna, C. J. *Nanotechnology* **2006**, *17*, 2783−2788.

(16) Perez, N.; Guardia, P.; Roca, A. G.; Morales, M. P.; Serna, C. J.; Iglesias, O.; Bartolome, F.; Garcia, L. M.; Batlle, X.; Labarta, A. *Nanotechnology* **2008**, *19*, 475704.

(17) Roca, A. G.; Marco, F. J.; Morales, M. P.; Serna, C. J. *J. Phys. Chem. C* **2007**, *111*, 18577−18584.

(18) Cannas, C.; Musinu, A.; Ardu, A.; Orrù, F.; Peddis, D.; Casu, M.; Sanna, R.; Angius, F.; Diaz, G.; Piccaluga, G. *Chem. Mater.* **2010**, *22*, 3353−3361.

(19) Slonczewski, J. C. *J. Appl. Phys.* **1961**, *32*, S253−S263.

(20) Moumen, N.; Bonville, P.; Pileni, M. P. *J. Phys. Chem.* **1996**, *100*, 14410−14416.

(21) Zeng, H.; Sun, S.; Vedantam, T. S.; Liu, J. P.; Dai, Z. R.; Wang, Z. L. *Appl. Phys. Lett.* **2002**, *80*, 2583−2585.
(22) Hansen, M. F.; Mørup, S. *J. Magn. Magn. Mater.* **1999**, *203*, 214−216.
(23) Del Bianco, L.; Fiorani, D.; Testa, A. M.; Bonetti, E.; Savini, L.; Signoretti, S. *Phys. Rev. B* **2002**, *66*, 174418−174429.
(24) Hansen, M. F.; Mørup, S. *J. Magn. Magn. Mater.* **1998**, *184*, 262−274.
(25) Peddis, D.; Cannas, C.; Musinu, A.; Piccaluga, G. *J. Phys. Chem. C* **2008**, *112*, 5141−5147.
(26) Kelly, P. E.; Grady, K. O.; Mayo, P. I.; Chantrell, R. W. *IEEE Trans. Magn.* **1989**, *25*, 3881−3883.
(27) Tronc, E.; Prenè, P.; Jolivet, J. P.; Dormann, J. L.; Grenèche, J. M. *Hyperfine Interact.* **1997**, *112*, 97−100.
(28) Cannas, C.; Musinu, A.; Piccaluga, G.; Fiorani, D.; Peddis, D.; Rasmussen, H. K.; Mørup, S. *J. Chem. Phys.* **2006**, *125*, 164714.
(29) Usov, N. A.; Peschany, S. E. *J. Magn. Magn. Mater.* **1997**, *174*, 247−260.
(30) Geshev, J.; Mikhov, M.; Schmidt, J. E. *J. Appl. Phys.* **1999**, *85*, 7321−7327.
(31) Kodama, R. H.; Berkowitz, A. E.; McNiff, J. E. J.; Foner, S. *Phys. Rev. Lett.* **1996**, *77*, 394−397.
(32) Virden, A.; Wells, S.; O'Grady, K. *J. Magn. Magn. Mater.* **2007**, *316*, e768−e771.
(33) Pileni, M. P. *J. Phys. Chem. B* **2001**, *105*, 3358−3371.
(34) Morup, S.; Hansen, M. F.; Frandsen, C. *Beilstein J. Nanotechnol.* **2010**, *1*, 182−190.
(35) Saslow, W. M. *Phys. Rev. B* **1988**, *37*, 676.
(36) Peddis, D.; Cannas, C.; Piccaluga, G.; Agostinelli, E.; Fiorani, D. *Nanotechnology* **2010**, *21*, 125705.
(37) Martínez, B.; Obradors, X.; Balcells, L.; Rouanet, A.; Monty, C. *Phys. Rev. Lett.* **1998**, *80*, 181−184.
(38) Del Bianco, L.; Hernando, A.; Multigner, M.; Prados, C.; Sanchez-Lopez, J. C.; Fernandez, A.; Conde, C. F.; Conde, A. *J. Appl. Phys.* **1998**, *84*, 2189−2192.
(39) Nogues, J.; Skumryev, V.; Sort, J.; Stoyanov, S.; Givord, D. *Phys. Rev. Lett.* **2006**, *97*, 157203−157204.